Ionizing Radiation Detector for Environmental Awareness in FPGA-Based Flight Computers

Todd Buerkle, Brock J. LaMeres, *Senior Member, IEEE*, Todd Kaiser, *Member, IEEE*, Eric Gowens, Laurie Smoot, Tiffany Heetderks, Katie Schipf, Lizzy Clem, Steph Schielke, and Rachael Luhr

***Abstract*— Ionizing radiation has a detrimental effect on digital electronics which need to operate in extraterrestrial environments. Modern reconfigurable digital fabrics are enabling new architectures for flight computers, which can exploit environmental awareness to increase their fault tolerance. In this paper, we present the design, modeling, and characterization of a radiation sensor which can be coupled with a reprogrammable hardware fabric to provide spatial information about radiation events that can cause logical faults. The sensor uses a wide area PN junction as its fundamental sensing element. As radiation passes through the sensor, electron hole pairs are created. The internal electric field of the PN junction sweeps the charge carriers in opposite directions which are ultimately sensed by orthogonally placed electrodes on the top and bottom of the sensor. This XY grid provides the spatial location of an ionizing radiation strike, which can be fed to the coupled computer fabric for environmental awareness. A reverse bias voltage is applied to the sensor in order to fully deplete the substrate for maximum charge carrier generation. The sensor is designed to detect the spatial location of radiation strikes of energy levels, which can cause faults in commercial field programmable gate arrays substrates.**

***Index Terms*— Radiation sensors, radiation tolerant computing, silicon radiation detectors.**

I. Introduction

THE detrimental effects that ionizing radiation has on digital integrated circuits (ICs) can be classified into two categories; (1) Total Ionizing Doze and (2) Single Event Effects [1,2]. Both of these effects come from the same physical phenomenon of radiation particles passing through the semiconductor material and creating an ionized electron/hole pair. Total Ionizing Doze (TID) effects result from charge carriers getting trapped in the insulating material of a transistor. When an electron/hole pair is created by the radiation strike (typically low energy electrons and protons) the carriers attempt to move back together to find an electrostatic equilibrium. Due to a difference in mobility rates in the semiconductor material, charge carriers can get trapped in the insulating material of the device. This can lead to threshold shifting and increased leakage current and results in permanent damage to the device.

Single Event Effects (SEE) are radiation strikes (typically from heavy ions and high energy protons) that by themselves do not cause permanent damage to the materials in a device but do result in a charge accumulation in the diffusion region of the transistor. The ionization of the diffusion region causes free charge to be created. If this charge has a large enough magnitude, it will produce a voltage that can be observed as a state change by a receiving gate. This type of event, known as a Single-Event Transient (SET) can lead to a logical failure called a Single-Event-Upset (SEU) if the state change is captured in a digital storage device. SETs and SEUs are referred to as soft faults because no permanent damage is caused in the circuit [3,4]. TID effects are typically handled using process modifications while SEEs are typically addressed using a logical fault mitigation approach [5]. There is great interest by the aerospace community in improving the fault mitigation strategies currently deployed to provided increased reliability and faster recover times.

The use of Field Programmable Gate Arrays (FPGAs) as the hardware fabric for military and aerospace computers has received great attention recently due to the improved computational performance that can be achieved and the inherent flexibility of the device [6,7]. The ability to dynamically reconfigure during a mission makes the practical deployment of high performance, reconfigurable computers a reality [8,9]. Internal modularity through the use of a many-core architecture further increases the capability of these computers.

In this paper, we describe the design of a sensor which can detect the position of ionizing radiation strikes with energy levels sufficient to cause single event effects in modern digital electronics (high energy protons, alpha particles and heavy ions). This sensor is designed for integration with a many-tile computing system implemented on an FPGA to provide environmental information to the computer in order to improve its fault tolerance. The XY location of ionizing radiation strikes are passed to the computer and used to spatially avoid and repair potentially faulted regions of the computer fabric. An overview of the tile-based computer system is given in section II. Section III presents the design and modeling of

Manuscript received December 19, 2011; revised January 24, 2012; accepted January 24, 2012. Date of publication January 31, 2012; date of current version April 27, 2012. This work was supported in part by NASA under Grant NNX10AN32A and Grant NNX10AN91A. The associate editor coordinating the review of this paper and approving it for publication was Prof. Evgeny Katz.

T. Buerkle, B. J. LaMeres, T. Kaiser, L. Smoot, T. Heetderks, K. Schipf, L. Clem, S. Schielke, and R. Luhr are with the Department of Electrical and Computer Engineering, Montana State University, Bozeman, MT 59717 USA (e-mail: toddbuerkle@gmail.com; lameres@ece.montana.edu; tjkaiser@ece.montana.edu; laurie.smoot@gmail.com; tiffany.heetderks@msu.montana.edu; schipfer779@hotmail.com; lizi.clem@gmail.com; stephani.schielke@gmail.com; rachael.luhr@msu.montana.edu).

E. Gowens is with the Radiation Testing Department, SEAKR Inc., Centennial, CO 80111 USA (e-mail: eric.gowens@gmail.com).

Color versions of one or more of the figures in this paper are available online at http://ieeexplore.ieee.org.

Digital Object Identifier 10.1109/JSEN.2012.2186288

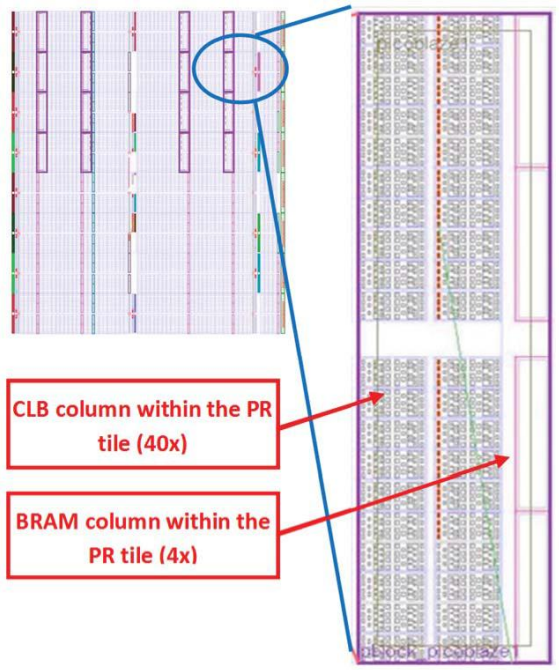

Fig. 1. Floor plan for the V5-LX110 FPGA highlighting the 16 reconfigurable tiles, each containing a PicoBlaze processor in addition to a zoomed in view of the PR showing the combinational logic blocks (CLB) and the block RAM (BRAM).

the sensor system. Sections IV and V presents the fabrication and characterization of the sensor respectively. Conclusions are given in Section VI.

II. Overview of Many-Core Architecture

Our research group at Montana State University has developed a many-core computer architecture implemented on an FPGA which can exploit environmental information from the spatial radiation sensor. In our approach, an FPGA fabric is divided into equally sized homogenous *tiles*. Each tile is sized such that it can contain an entire soft processor and be partially reconfigured (Fig. 1.). Partial reconfiguration (PR) involves reprogramming only a section of the FPGA (i.e., 1 tile). PR has the effect of both restoring the initial contents of the configuration memory and inherently resetting the circuitry in the tile. This repairs faults that occur in either the main circuit fabric of the tile or in its corresponding configuration memory.

At any given time, three of the soft processors are configured in triple modular redundancy (TMR) with the rest of the processors available as spares. TMR detects faults by voting on the output of three identical circuits. This not only produces the correct output in the event of a fault but also indicates which of the tiles has been faulted. In the event that the TMR voter detects a fault, the system allows the two good processors to complete their current task and then conducts a repair procedure which replaces the faulted processor with a spare tile. Once the spare is brought online and reinitialized, the three processors continue foreground operation while PR is conducted on the faulted tile in the background. The repaired tile is then reintroduced into the system as a spare.

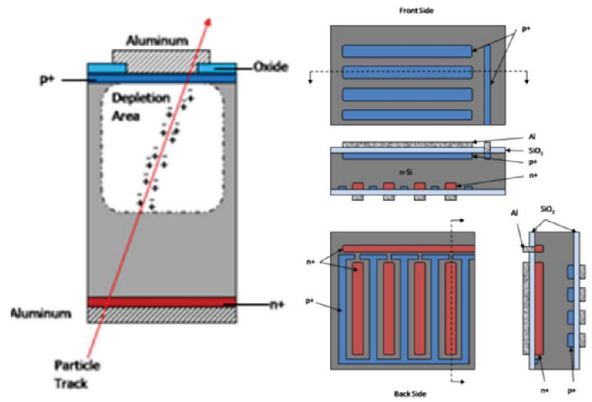

Fig. 2. Cross-section of a model radiation detector and layout of the front- and back-side strips.

In addition, a system runs in the background comparing the contents of the FPGA's configuration memory with an original golden copy which resides in a non-volatile memory device off-chip. This circuit, known as a *scrubber*, can detect faults that occur in the configuration memory of spare tiles and perform PR before the spare is brought online. The computer architecture described has been prototyped on both a Xilinx Virtex-5 and Virtex-6 FPGA using the Xilinx *picoBlaze* soft processor [10].

III. Sensor Design

A. Theory of Operation

A sensor has been designed based on techniques and practices developed for use in nuclear spectroscopy experiments. In the field of elementary particle physics it is necessary to take very fast and precise position measurements to monitor very rare and short lived ionizing particles produced in particle colliders [11-14]. Semiconductor radiation sensors have been developed to monitor the paths of these particles as they exit a reaction. Conversely, this design uses the same techniques to monitor the position of ionizing radiation as it enters electronics for space systems. This sensor is designed to sense high energy radiation such as trapped protons, alpha particles and heavy ions. These particles produce the greatest ionization in the sensor and are capable of easily traversing the entire thickness of the sensor.

Fig. 2 shows a cross-section of the fundamental sensing element, a PN junction used as a radiation detector. The ionizing radiation passes through the sensor creating electron hole pairs at an average rate of 3.3 eV per electron-hole pair. In silicon, 1 MeV of energy transferred corresponds to 48.4 fC of charge produced, which is more than enough to flip the state of a logic circuit fabricated with modern processes [11-14]. Within a diffusion length of the depletion region, the intrinsic electric field sweeps the charges toward their corresponding electrodes, electrons to the N+ side of the substrate and holes to the opposite P+ side. The energy of the radiation and the size of the depletion region determine the amount of charge ultimately collected.

The design selected utilizes double sided strip detectors. The strip detector is used as the basis for this design because of

its simplicity, speed and ease of production without sacrificing position resolution [15,16]. The principle of the strip detector is very simple. It is based on a large area PN diode, very similar to a solar cell. The difference stems from the electrodes in the radiation sensor, which are broken up into narrow strips running orthogonal to each other on both sides of the substrate, each of them being read-out as a separate electronic channel. When charge is created in the sensor, it diffuses to the front and back of the device and is collected on the closest strip. The location of the ionizing radiation strike is determined by the intersection of the front and back strips.

B. Modeling

The sensor substrate is intrinsic silicon. The sensor is composed of a front side doped with p+ material (boron) and a back side doped with n+ material (phosphorous). These dopants create the desired charge collection region for the strip detector. For this design, high doping concentration on the front and back surfaces of the wafers is desired. These high surface concentrations produce two results. The first result is that a high doping concentration allows for a better electrical connection between the doped regions and the aluminum contacts. This ohmic connection greatly reduces the series resistance in the device and eliminates one potential area for losses. The second effect of a high surface doping concentration is that the depletion regions are pushed to a maximum depth into the bulk silicon wafer. By increasing the depth of the depletion regions, the active area of the sensor capable of collecting electrons and holes is expanded.

In order to determine the active sensing area, the size of the depletion regions needs to be calculated. These active areas provide an idea as to how much charge is collected for a given radiation strike, such as a heavy ion. The size of the depletion region directly depends on the doping concentrations achieved during fabrication. Measuring the sheet resistivity of the completed devices provides a means to calculate these doping concentrations. Using (1), the resistivity of the doped sensor strips is determined from the measured sheet resistivities.

$$\rho_{P/N} = R \cdot X \tag{1}$$

In (1), R is the measured sheet resistivity and X is the final junction depth of the dopants after the completion of the fabrication process. With these resistivities determined, a table is used to find the actual doping concentration achieved during fabrication. Once these concentrations are known, the built in voltage is calculated by (2).

$$V_{bi} = \frac{kT}{q} \ln\left(\frac{N_J N_D}{n_i}\right) \tag{2}$$

In (2), k is Boltzmann's constant, T is the temperature in Kelvin, q is the charge on an electron, N_D is the background donor concentration, and $n_i = 1.45{*}10^{10}$ cm^{-3} (intrinsic concentration of the silicon wafer). The value for N_J is either the P+ or N+ doping concentration that was previously determined. These built in voltages produce two depletion regions inside of the silicon wafer. These widths determine the active region of the sensor. In order to determine the active area, (3) is used when no bias is applied to the sensor.

$$w_{no\_BIAS} = \sqrt{\frac{2\varepsilon_r \varepsilon_o (N_J + N_D)}{q N_J N_D}(V_{bi})} \tag{3}$$

In (3), $\varepsilon_r = 11.9$, ε_o is the permittivity of free space, and V_{bi} is the previously calculated built in voltage.

Typical doping concentrations produce depletion regions that cover some percentage of the total sensor thickness. These result in a collection area for the cell that is less than the total thickness, meaning that some of the charge produced by an ionizing radiation strike is not collected and is lost to recombination. These losses can be compensated for by applying a reverse bias voltage to the pn junction. This voltage is applied as a negative voltage to the top (P+) side of the sensor. Using (4) shows how the depletion widths are changed when a bias is applied to the junction.

$$w_{BIAS} = \sqrt{\frac{2\varepsilon_r \varepsilon_o (N_J + N_D)}{q N_J N_D}(V_{bi} - V_{BIAS})} \tag{4}$$

Applying a large reverse bias causes the depletion regions to grow. By applying the correct bias, the depletion regions are stretched across the entire thickness of the wafer. This gives the maximum collection of EHPs and the best overall performance for the radiation sensor.

With this increased depletion region size, applied bias voltage, and built in voltage known, the internal electric field is calculated in (5).

$$\vec{E} = -\nabla V \approx \frac{V_{bi} + V_{BIAS}}{w_{BIAS}} \tag{5}$$

This electric field is produced by the built in voltage being applied across the thickness of the depletion width. If an electron hole pair is produced inside of a depletion region, these charges are immediately separated by the electric field. This separation results from the force exhibited by the electric field on charged particles such as electrons and holes. The velocity of these charge carriers due to the electric field can be determined in (6), where μ is the mobility of the electrons or the holes.

$$\vec{v}(x) = \mu \cdot \vec{E} \tag{6}$$

Once separated, these charges are collected at the electrodes on the front and back of the sensor. The time before the electron and holes are collected depends on the location of their respective generation. Using this path length, the carrier velocity, and (7), the charge carrier transient time is computed.

$$Transient\_Time = \frac{Collection\_Path\_Length}{Velocity} \tag{7}$$

Once the charge transient time is known, the current can be found if the amount of charge produced inside of the depletion region is known. In order to determine the charge generated, the energy of the incoming heavy ion must be known. For most available radiation sources, the linear energy transfer (LET) of the particle is known. This value is used to quantify the effects of ionizing radiation on materials and is a measure of the energy transferred to a material as an ionizing particle

passes through it. For this design, the LET is a measurement of the energy transferred to the silicon lattice from the high energy heavy ion.

For a known LET, the charge produced inside the sensor is determined with (8).

$$Q = \frac{LET \cdot \rho \cdot q \cdot t}{3.3} \tag{8}$$

In (8), LET is the linear energy transfer for a given radiation source in eV·cm^2/mg, ρ is the density of the target material in mg/cm^3, q is the charge on an electron, t is the thickness of the sensor (0.03 cm in this case) in cm, and the factor 3.3 is the electron hole pair generation rate inside of silicon in EHPs/eV. In general, a LET profile is available for a given heavy ion and the desired target material. This means that (8) allows for the calculation of the charge profile inside of the entire radiation sensor. Once the charge at a certain location and the transient time from that location until collection is known, the current out of the radiation sensor is determined by (9).

$$I = \frac{Q}{Transient\_Time} \tag{9}$$

The design is completed with these parameters in mind in order to maximize the electron hole pair generation and collection for the radiation sensor when struck by a heavy ion.

IV. Sensor Fabrication

The dimensions of the die for the sensor are 20 mm × 20 mm to accommodate all Xilinx FPGA chip sizes. These dimensions ensure that the sensor can completely cover the die used in the FPGA. This sensor design has 16 front side and 16 back side channels. The back side channels are rotated 90° with respect to the front side channels. The front and back side channel width is 1mm and the spacing between adjacent channels is 0.1 mm. The length of each channel is 18.7 mm. This produced an active sensing area of 18.7 mm^2. Also included on the front side of the sensor are bias rings. The purpose of these rings is to stabilize the long term performance of the sensors. The need for these rings arises from the fact that fully depleted silicon sensors suffer from charge build up on oxide surfaces. This charge build up can affect the depletion region and eventually produce a reverse current opposing the desired flow of electrons. The bias rings act as a series of MOSFETs with the gates and sources connected. This series gradually decreases the bias voltage towards the edges of the sensor. The inclusion of these rings improves the long term performance of the radiation sensors.

The orthogonal grid of channels produces 256 unique pixels that can be stimulated by a radiation strike. Signals are then collected on each side of the sensor, giving the X and Y coordinates of the incoming strike. The top of the sensor produces the X coordinates and the back side outputs the Y coordinates. These coordinates are then input into an FPGA based computer system created with redundant tiles arranged in a grid. Based on the strike location, the computer system takes the necessary actions to reconfigure the active tiles and avoid the location of the radiation strike. This ensures that only undamaged tiles are used by the system and eliminates potential faults caused by the radiation strike.

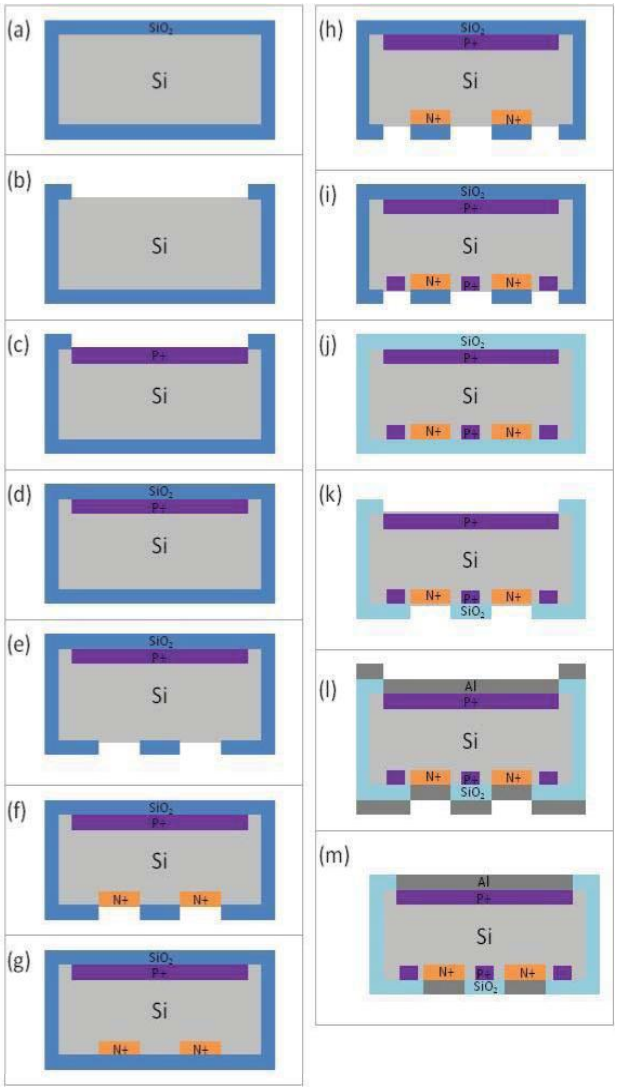

Fig. 3. Process steps (a)–(m) to create the radiation sensor.

A 100 mm diameter, 300 μm thick, intrinsic silicon wafer with a <100> crystal orientation is selected as the substrate for the radiation sensor. The first step in the process involves growing a masking layer around the wafer. This oxidation process is a wet process, meaning that water vapor is used to grow the oxide layer. This produces a SiO_2 layer that is 0.5 μm thick (Fig. 3(a)). Next, photolithography is performed using a dark field mask. This mask is used to produce the front side P+ (boron) doping regions. The wafer is patterned and the regions of the front side strips are etched (Fig. 3(b)).

The front side is now doped with boron (Fig. 3(c)). The remaining oxide is removed using a BOE bath and a new layer of oxide is grown using the same method as previously described (Fig. 3(d)). Photolithography is performed to produce the regions for the back side N+ (phosphorous) doping. The wafer is patterned and etched to produce the back side strips (Fig. 3(e)). The back side is doped with phosphorous (Fig. 3(f)). Again, the remaining oxide is removed and a new layer is grown using the oxidation furnace (Fig. 3(g)).

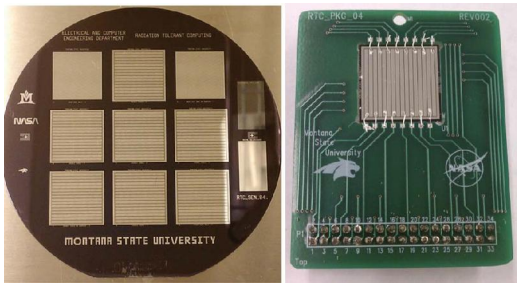

(a) (b)

Fig. 4. Fabricated radiation sensor. (a) Whole wafer. (b) Packaged radiation sensor.

The next step is another photolithography process. This photolithography step is used to create the back side barrier diffusion regions. The back side of the wafer is patterned and etched as before (Fig. 3(h)). The back side barrier regions are doped with boron (P+ material). These barrier diffusions are included to limit the charge coupling between adjacent strips on the back side of the sensor. The bulk of the sensor is slightly N-type which leads to coupling between the back side strips if these barrier diffusions are not included to electrically isolate adjacent channels (Fig. 3(i)). The remaining oxide is then removed using BOE.

The next step in the fabrication process involves growing a layer of dry oxide. In this oxidation, water vapor is not used to aide in the growth of the SiO_2 layer. Oxygen gas flow is the catalyst that produced this layer of oxide. This oxidation produced a layer of oxide that is 90 nm thick (Fig. 3(j)). Photolithography is then performed on the front and the back of the wafer. This process is used to produce regions for the metal contacts to the front and back side strips of the sensor. The front and back side strips are patterned and etched (Fig. 3(k)).

Aluminum is then deposited on the front and back of the wafer using a physical vapor deposition (PVD) process. The aluminum sample that is evaporated was 36 cm^2 for both the front and the back surfaces (Fig. 3(l)). Photolithography is then used to pattern this front and back side metal. This step leaves only the contact aluminum on the surfaces of the wafer. The wafer is patterned and etched for the last time in the process (Fig. 3(m)). To complete the fabrication process, the wafers are annealed for 30 minutes at 400 °C. This annealing process improves the electrical connection between the deposited aluminum and the doped silicon regions. A low series resistance at these junctions is essential for this design. Nine different sensors are created on each wafer. The individual sensors are separated using a wafer saw. Fig. 4 shows the wafer after fabrication and an individual radiation sensor packaged in the custom printed circuit board.

V. Sensor Performance

A. Calculating Sensor Parameters

The sensors are fabricated using the previous process. The expected performance is then determined using a combination of measured and calculated sensor parameters. The wafers used for the sensor fabrication have a light background concentration of donor atoms. The vendor specified this background concentration to be $N_D = 2.15{*}10^{11}$ atoms/cm^3. The maximum doping concentration achievable by the sources available is $N_{D+} = 1.20{*}10^{20}$ atoms/cm^3 for the P+ doping and $N_{A+} = 2.2{*}10^{20}$ atoms/cm^3 for the N+ doping. The actual doping achieved will be less than these maximums and can be calculated using the measured sheet resistivity of the devices. The sheet resistivity of one of the fabricated sensors is measured using a JANDEL four point probe. The measured sheet resistivities are $R_{P+} = 46.07\ \Omega/\square$ and $R_{N+} = 11.46\ \Omega/\square$.

TABLE I
Parameters to Calculate Active Sensing Size

Symbol	Quantity	Value
R_{P+}	P+ sheet resistivity	46.07 Ω/□
R_{N+}	N+ sheet resistivity	11.46 Ω/□
X_{P+}	P+ doping junction depth	$1.691{*}10^{-4}$ cm
X_{N+}	N+ doping junction depth	$1.335{*}10^{-4}$ cm
ρ_{P+}	P+ resistivity	$7.79{*}10^{-3}\Omega{\cdot}$cm
ρ_{N+}	N+ resistivity	$1.53{*}10^{-3}\Omega{\cdot}$cm
N_{P+}	P+ doping concentration	$1.15{*}10^{19}$ cm^{-3}
N_{N+}	N+ doping concentration	$4.53{*}10^{19}$ cm^{-3}
V_{bi-P+}	Front side built in voltage	0.619 V
V_{bi-N+}	Back side built in voltage	0.655 V
w_{P+}	Front side depletion width	61.57 μm
w_{N+}	Back side depletion width	63.31 μm

The fabrication process sets the final junction depth for the front and back side dopants since each thermal process causes the dopants to diffuse further into the silicon wafer. The doping times and temperatures are designed so that the final junction depth is less that 2 μm. This ensures meeting the requirement of high surface doping concentrations. The junction depths calculated from the fabrication process are $X_{P+} = 1.691{*}10^{-4}$ cm and $X_{N+} = 1.335{*}10^{-4}$ cm. Using the measured sheet resistivities, the final junction depths, and (1) – (6), the radiation sensor parameters are calculated for this design. These values can be seen in Table I.

These depletion widths are the active charge collecting areas of the fabricated radiation sensor. Without applying an external reverse bias, approximately 125 μm of the sensor thickness can be used to collect the charge produce by an ionizing radiation strike. This limited active area is based on the assumption that the diffusion length of the carriers is very short inside the sensor. Fig. 5 shows the depletion regions produced by the doping concentrations in the sensor.

B. Simulated Heavy Ion Strike

In order to evaluated whether the sensor will operate in its target environment, the parameters for a krypton (Kr) heavy ion at 25 MeV/amu were used to calculate the output current of the sensor. This particle gives a total ion energy of 2081 MeV (energy times mass in amu) and has the ability to pass through the entire sensor thickness. This heavy ion has an energy that is a reasonable approximation of the radiation that this sensor would see in a low earth orbit in addition to being available at a number of cyclotrons for future chamber testing.

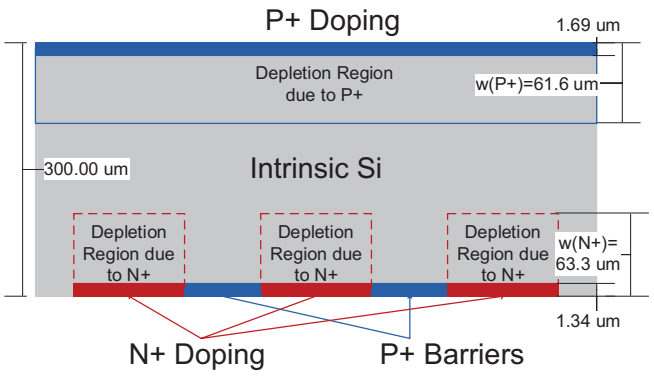

Fig. 5. Cross section of the design radiation sensor.

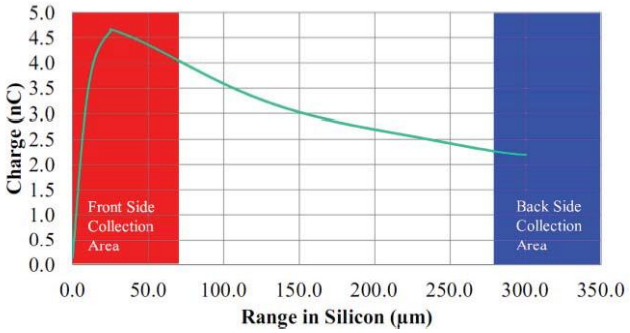

Fig. 6. Charge profile produced when a 25 A MeV Kr atom passes through the sensor.

As a krypton ion enters the radiation sensor, the particle transfers energy to the sensor and creates electron hole pairs based on LET for this krypton ion. The LET for this ion was provided by the Texas A&M Radiation Effects Facility. The charge profile calculated for this ion as it penetrates the sensor is determined using (8) and can be seen in Fig. 6. The charge produced will only be collected in the depletion region widths which are found using (4). These regions are shown in Fig. 6 as the highlighted sections.

Using (5)–(9), the currents produced in the two depletion regions, due to the krypton atom strike, are calculated. Table II shows the additional sensor parameters calculated in order to determine these currents. The velocities in Table II are used in (7) to determine the transient times for both of these carries as a function of position in the sensor. Finally, using the charge at a given sensor position and the transient time to collection for that location, the current is found for the electrons and holes using (9). Fig. 7 and 8 show the currents generated by this simulated high energy krypton atom strike.

C. IR Laser Testing

A 1064 nm wavelength infrared (IR) laser was used to stimulate the sensor to verify functional operation. At this wavelength silicon has an absorption coefficient that allowed the IR radiation to penetrate to the opposite side of the sensor. This enabled a high energy stimulation of both front and back side channels simultaneously to verify the electron hole pair generation of the sensor and the XY positional detection. Instead of kinetic energy being transferred by the radiation particle to the silicon lattice, this test utilized optical absorption to generate the electron hole pairs. At a wavelength of 1064 nm, the IR laser had an energy of approximately 1.168 eV. This was greater than the band gap of silicon (1.12 eV) and allowed the IR laser to be used to generate electron-hole pairs in the silicon based radiation sensor.

The sensor was stimulated with the laser and the magnitudes of the front and back side channels were observed on a digital multi-meter. The laser was aimed at a distinct location and the data for those coordinates was collected. A 30 V reverse bias was applied to the sensor electronics during these measurements. This bias voltage expanded the depletion region to cover the entire thickness of the wafer. By expanding the depletion width, the electron and hole collection for the sensor was increased and a stronger output signal was achieved. The output voltages for all of the front and back side channels were recorded. These voltages can then be used to determine the current output from the sensor. Fig. 9 shows the sensor system response when struck in XY location 9×9. This refers

TABLE II
PARAMETERS TO CALCULATE SENSOR CURRENT

Symbol	Quantity	Value
μ_h	Hole mobility	470.46 cm^2/V-s
μ_e	Electron mobility	1413.87 cm^2/V-s
E_{P+}	Front side electric field	100.54 V/cm
E_{N+}	Back side electric field	103.46 V/cm
v_h	Hole velocity	47300 cm/s
v_e	Electron Velocity	146279 cm/s

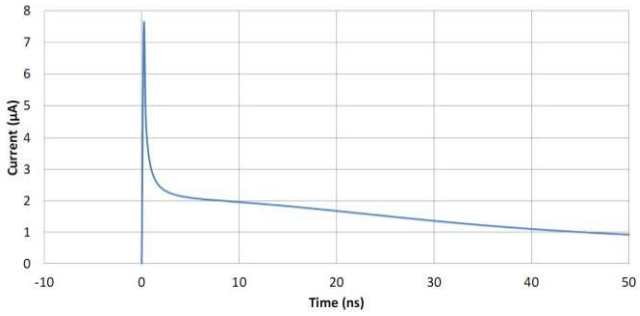

Fig. 7. Front side current (holes) produced from a Kr ion strike.

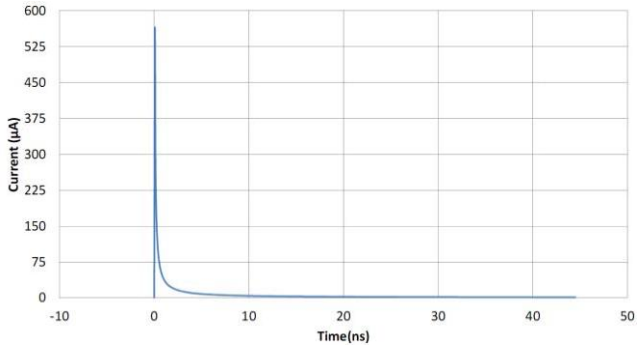

Fig. 8. Back side current (electrons) produced from a Kr ion strike.

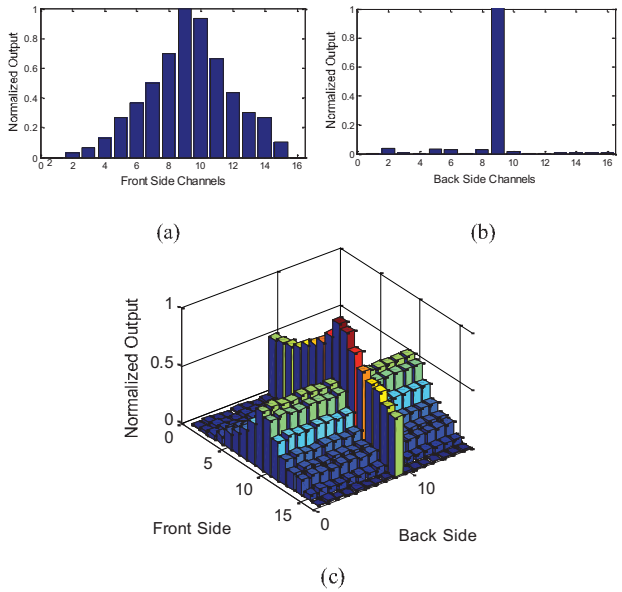

Fig. 9. Normalized sensor response to IR laser when struck at XY position 9×9 and measured at the top and bottom sensor electrodes. (a) Front-side channel response. (b) Back-side response. (c) Combined XY data, which is used to produce the exact strike location.

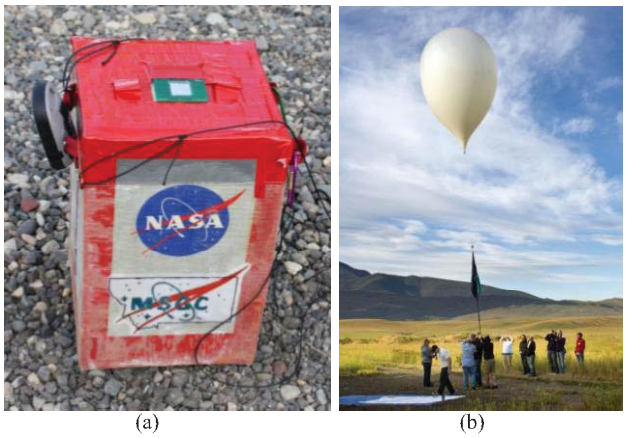

Fig. 10. Payload design and balloon system used to conduct high altitude testing on a balloon system. (a) Payload containing the data logging electronics and sensor attached on top. (b) Payload being launched on the high altitude balloon platform.

to striking the sensor as close to the center as possible which corresponds to front-side channel 9 and backside channel 9.

D. High Altitude Balloon Testing

As an additional test, a payload was designed to power the sensor and log radiation strike data in a high altitude environment. At altitudes up to 100,000 feet, high energy ($>$ 10 MeV) particle fluxes can be as high as hundreds of particles per second. The goal of this payload was to expose the sensor to these particles and record the total number of strikes observed throughout the duration of the flight. The XY location of the radiation strikes was not determined during this test because this experiment was simply designed to test the ability of the radiation sensor to generate useable output signals when struck by an ionizing radiation particle.

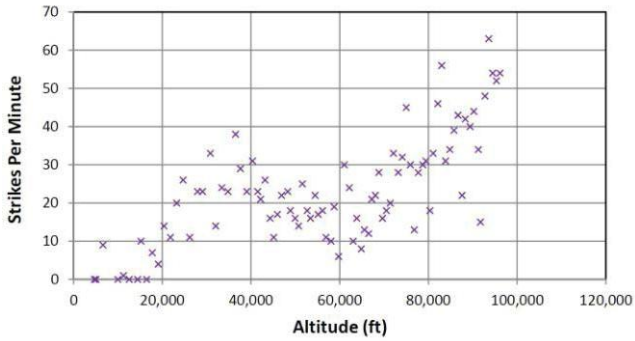

Fig. 11. Radiation data collected from the sensor system from a high altitude balloon flight conducted in Southwest Montana.

Future testing will be conducted to determine the XY decoding capability of the radiation sensor.

The payload is shown in Fig. 10(a). The sensor resides on the top outside of the insulating structure which contains the electronics. The sensor system was flown on a high altitude balloon system to a height of 97,237 feet. The balloon system was administered by the Montana Space Grant Consortium which routinely conducts flights in Southwest Montana. The balloon system is shown in Fig. 10(b).

The flight lasted 89 minutes. Data was logged for the duration of the flight. Fig. 11 shows the number of strikes recorded by the sensor system as a function of altitude. This figure shows that the sensor system performed as expected. The number of radiation strikes increased steadily as it rose in altitude.

VI. Conclusion

We presented the design, fabrication and characterization of a positional sensor for use in detecting ionizing radiation. The sensor was designed for use with an FPGA-based flight computer to provide environmental information in order to improve the computer's fault tolerance when in harsh radiation environments. The sensor was tested using an IR laser and also flown on a high altitude balloon. Both tests showed that the sensor operated as designed and was indeed capable of sensing high energy radiation strikes. By providing spatial awareness of potential ionizing radiation strikes to flight computers, more robust fault mitigation strategies can be deployed.

Acknowledgment

The authors would like to thank NASA, Washington D.C., and the Montana Space Grant Consortium, NASA, for supporting this paper.

References

[1] C. Claeys and E. Simoen, *Radiation Effects in Advanced Semiconductor Materials and Devices*. Berlin, Germany: Springer-Verlag, 2002.
[2] A. Holmes-Siedle and L. Adams, *Handbook of Radiation Effects*, 2nd ed. New York: Oxford Univ. Press, 2002.
[3] M. Stetller, "Radiation effects and mitigation strategies for modern FPGAs," in *Proc. 10th Annu. Workshop LHC Future Experim.*, 2004, pp. 1–5.
[4] R. W. Butler, "A primer on architectural level fault tolerance," NASA, Washington D.C., Tech. Rep. NASA/TM-2008-215108, Feb. 2008.

[5] A. Keys, J. Adams, R. Darty, M. Patrick, M. Johnson, and J. Cressier, "Radiation hardened electronics for space environments (RHESE) project overview," presented at the International Planetary Probes Workshop, Atlanta, GA, Jun. 2008.
[6] K. Underwood, "FPGAs versus CPUs: Trends in peak floating-point performance," in *Proc. FPGA*, Monterey, CA, Feb. 2004, pp. 1–10.
[7] S. Hauck, "The roles of FPGAs in reprogrammable systems," *Proc. IEEE*, vol. 86, no. 4, pp. 615–638, Apr. 1998.
[8] T. J. Todman, G. Constantinides, S. J. E. Wilton, O. Mencer, W. Luk, and P. Y. K. Cheung, "Reconfigurable computing: Architectures and design methods," *IEE Proc.-Comput. Digital Tech.*, vol. 152, no. 2, pp. 193–207, Mar. 2005.
[9] C. Chang, J. Wawrzynek, and R. W. Brodersen, "BEE2: A high-end reconfigurable computing system," *IEEE Design Test Comput.*, vol. 22, no. 2, pp. 114–125, Mar.–Apr. 2005.
[10] *PicoBlaze 8-bit Embedded Microcontroller User Guide Xilinx UG129 (v2.0)*. (2010, Jan.) [Online]. Available: http://www.xilinx.com/
[11] G. Lutz, *Semiconductor Radiation Detectors*. New York: Springer-Verlag, 1999.
[12] L. Rossi, P. Fischer, T. Rohe, and N. Wermes, *Particle Acceleration and Detection: Pixel Detectors from Fundamentals to Applications*. New York: Springer-Verlag, 2006.
[13] J. Kemmer and G. Lutz, "New structures for position sensitive semiconductor detectors," *Nucl. Instrum. Methods Phys. Res. A*, vol. 273, nos. 2–3, pp. 588–598, Dec. 1988.
[14] S. Seidel, "A review of design considerations for the sensor matrix in semiconductor pixel detectors for tracking in particle physics experiments," *Nucl. Instrum. Methods Phys. Res. A*, vol. 465, nos. 2–3, pp. 267–296, 2001.
[15] M. Turala, "Silicon tracking detectors-historical overview," *Nucl. Instrum. Methods Phys. Res.*, vol. 541, nos. 1–2, pp. 1–14, 2005.
[16] H. Dijkstra, "Overview of silicon detectors," *Nucl. Instrum. Methods Phys. Res.*, vol. 494, nos. 1–2, pp. 86–93, Feb. 2002.

Todd Buerkle received the B.S. degree in electrical engineering from Montana State University, Bozeman, in 2010. He is currently pursuing the Masters degree in electrical engineering with the Department of Electrical and Computer Engineering, Montana State University.

Brock J. LaMeres (M'98–SM'09) received the B.S. degree in electrical engineering from Montana State University, Bozeman, in 1998, the M.S. degree in electrical engineering from the University of Colorado, Colorado Springs, in 2001, and the Ph.D. degree in electrical engineering from the University of Colorado, Boulder, in 2005.

He is currently an Assistant Professor with the Department of Electrical and Computer Engineering, Montana State University, where his research focuses on digital systems.

Todd Kaiser (M'00) received the B.S. degree in physics from Montana State University, Bozeman, in 1981, the M.S. degree in physics from Oregon State University, Corvallis, in 1984, and the Ph.D. degree in electrical engineering from the Georgia Institute of Technology, Atlanta, in 2000.

He is currently an Associate Professor with the Department of Electrical and Computer Engineering, Montana State University.

Eric Gowens received the B.S. and M.S. degrees in electrical engineering from Montana State University, Bozeman, in 2009 and 2011, respectively.

He is currently a Radiation Effects Engineer with SEAKR Inc., Centennial, CO.

Laurie Smoot is currently pursuing the Bachelors degree with the Department of Electrical and Computer Engineering, Montana State University, Bozeman.

Tiffany Heetderks is currently pursuing the Bachelors degree with the Department of Electrical and Computer Engineering, Montana State University, Bozeman.

Katie Schipf is currently pursuing the Bachelors degree with the Department of Mechanical Engineering, Montana State University, Bozeman.

Lizzy Clem is currently pursuing the Bachelors degree with the Department of Mechanical Engineering, Montana State University, Bozeman.

Steph Schielke is currently pursuing the Bachelors degree with the Department of Computer Science, Montana State University, Bozeman.

Rachael Luhr is currently pursuing the Bachelors degree with the Department of Computer Science, Montana State University, Bozeman.